



ELSEVIER

Available online at www.sciencedirect.com



C. R. Mecanique 333 (2005) 39–49



COMPTES RENDUS

MECANIQUE

<http://france.elsevier.com/direct/CRAS2B/>

High-Order Methods for the Numerical Simulation of Vortical and Turbulent Flows

High-order LES modeling of turbulent incompressible flow

Richard Pasquetti

Laboratoire J.A. Dieudonné, UMR CNRS 6621, université de Nice–Sophia Antipolis, parc Valrose, 06108 Nice cedex 02, France

Available online 4 January 2005

Abstract

This article presents the high-order algorithms that we have developed for large-eddy simulation of incompressible flows, and the results that have been obtained for the 3D turbulent wake of a cylinder at a Reynolds number of $Re = 3900$. **To cite this article:** R. Pasquetti, C. R. Mecanique 333 (2005).

© 2004 Académie des sciences. Published by Elsevier SAS. All rights reserved.

Résumé

Simulation des grandes échelles d'écoulements incompressibles turbulents par méthode d'ordre élevé. L'article présente les algorithmes d'ordre élevé que nous avons développés pour la simulation des grandes échelles d'écoulements incompressibles ainsi que les résultats obtenus pour le sillage 3D turbulent d'un cylindre à un nombre de Reynolds de $Re = 3900$. **Pour citer cet article :** R. Pasquetti, C. R. Mecanique 333 (2005).

© 2004 Académie des sciences. Published by Elsevier SAS. All rights reserved.

Keywords: Computational fluid mechanics; Large-eddy simulation; Spectral methods; Wake flows

Mots-clés : Mécanique des fluides numérique ; Simulation des grandes échelles ; Méthodes spectrales ; Ecoulements de type sillage

1. Introduction

Despite the amazing increase of the computer capacities and the efforts made to elaborate a complete theory of turbulence, the direct numerical simulation (DNS) and the statistical approaches, based on the Reynolds Averaged Navier–Stokes (RANS) equations, do not yet permit satisfactory computations of turbulent complex flows. Between DNS and RANS stands the large-eddy simulation (LES) approach, based on the idea of computing only the large eddies of the flow and to restrict the modeling to the smaller ones. This approach remains, and will probably for some time, adequate to compute turbulent flows. However, in order to clearly discern the numerical approximation errors and the sub-grid-scale (SGS) modeling, using high-order methods is from our point of view a fundamental requirement, especially to deal with some detailed studies of fluid dynamics.

E-mail address: Richard.Pasquetti@unice.fr (R. Pasquetti).

To compute 3D wakes in channel-like geometries with a homogeneous spanwise direction, we use a multi-domain Chebyshev–Fourier spectral approximation in space and a second order semi-Lagrangian projection method in time. The SGS model makes use of the so-called approximate deconvolution method (ADM) [1,2], which may be viewed as an extension of the scale similarity model [3]. In the framework of our numerical scheme but in the same spirit, we introduced in [4] the Defiltering–Transport–Filtering (DTF) algorithms. SGS models based on scale similarity are known to be better on a priori tests than those based on an eddy-viscosity, typically the Smagorinsky model (see e.g. [5]), possibly associated with the dynamic modeling [6]. However, they are also known to yield numerical instabilities, which may be overcome by combining in more or less empirical ways the scale similarity and eddy-viscosity concepts [7]. The approach that we propose is to use the DTF modeling, combined with the spectral vanishing viscosity (SVV) method to stabilize the calculations. The SVV method, first developed to solve non-linear hyperbolic equations, typically the Burgers equation, with the Fourier [8] or Legendre [9] spectral method, indeed shows the property to preserve the spectral accuracy of the approximation. Thus, the convergence of the numerical approximation toward the exact solution remains exponential, even, of course, if the convergence rate is worse with a SVV term than without. Note that the present approach should not be confused with those making use of a spectral viscosity, on the grounds of homogeneous and isotropic turbulence theory [10].

After the description, in Section 2, of the high-order scheme and of the associated LES modeling of turbulent inhomogeneous flows we present, in Section 3, the results that we have obtained for a classical benchmark: the turbulent wake of a cylinder, Reynolds number $Re = 3900$. We compare especially results obtained when using DTF, for the SGS modeling, stabilized with SVV with the no-SGS model approach making only use of SVV. We discuss these results in Section 4 and finally conclude in Section 5.

2. The spectral LES model

Along the streamwise direction we use a domain decomposition technique to efficiently handle the elongated geometries typically encountered when studying wake type flows. In each subdomain we use spectrally accurate approximations, based on Chebyshev polynomials in the x -streamwise and y -cross-flow directions and on Fourier series in the z -spanwise homogeneous direction. The time-scheme makes use of 3 steps: a transport step to handle the convective term, a diffusion term to handle the viscous term, and a projection step to finally obtain a divergence-free velocity field. The LES modeling, i.e. the DTF algorithm, is implemented in the transport step and the SVV stabilization technique in the diffusion step.

To model the bluff body, inside the channel, we use a smoothed penalty technique. Essentially, the smoothing is realized through a filtering of its characteristic function, as in [11], but now we use for the filtering an improved version of the ‘raised cosine filter’ in order to more precisely take into account the position of the bluff body. Such a modeling implies that spectral accuracy is lost, at least locally. Here we assume that the phenomenon remains local and thus does not drastically affect the flow, especially the far wake.

The equations that we have to solve are then the filtered Navier–Stokes equations with a body force term to model the bluff body. Denoting, as it is usual (see e.g. [5]), with an over bar the filtered quantities we assume that the large scales of the (incompressible) flow are governed by the dimensionless equations:

$$\overline{D_t \mathbf{u}} = -\nabla \bar{p} + \frac{1}{Re} \nabla^2 \bar{\mathbf{u}} + \bar{\mathbf{f}} \quad (1)$$

$$\nabla \cdot \bar{\mathbf{u}} = 0 \quad (2)$$

with D_t the material derivative and t the time, \mathbf{u} the velocity field, p the pressure, \mathbf{f} a force term and Re the Reynolds number.

Let us now describe briefly the different steps of the algorithm, together with the implementation of the LES modeling (more details may be found in [12]). For the sake of simplicity in the notations but also to clearly outline

that the diffusion and projection steps are similar to those of the DNS implementation, we omit the over bars in their descriptions.

2.1. Transport step and DTF algorithm

The approximation of the material derivative with a BE Q (backward Euler of order Q) scheme yields, with α_q , $q = 0, \dots, Q$ a set of given coefficients:

$$D_t \mathbf{u}(t_{n+1}) = \frac{1}{\Delta t} \left(\alpha_0 \mathbf{u}^{n+1} + \sum_{q=1}^{q=Q} \alpha_q \tilde{\mathbf{u}}^{n+1-q} \right) + O(\Delta t^Q)$$

with $\mathbf{u}^{n+1} \approx \mathbf{u}(\mathbf{x}, t_{n+1})$ and $\tilde{\mathbf{u}}^{n+1-q} \approx \mathbf{u}(\chi(\mathbf{x}, t_{n+1}; t_{n+1-q}), t_{n+1-q})$, where $\chi(\mathbf{x}, t_{n+1}; t)$ solves the characteristics equation stemming from (\mathbf{x}, t_{n+1}) . To compute the $\tilde{\mathbf{u}}^{n+1-q}$, the natural approach is then to determine for each mesh-point \mathbf{x}_k the value of the velocity \mathbf{u} at the times $\{t_n, t_{n-1}, \dots, t_{n+1-Q}\}$ and at the points $\chi(\mathbf{x}_k, t_{n+1}; t_{n+1-q})$, $q = 1, \dots, Q$. However, the ‘method of characteristics’ cannot be used in the framework of standard spectral methods because high-order interpolations would be too expensive and, moreover, would yield numerical instabilities. To overcome this difficulty we use an ‘Operator Integration Factor’ (OIF) semi-Lagrangian method [13–15]. The basic idea is here to transport the $\mathbf{u}^{n+1-q}(\chi(\mathbf{x}_k, t_{n+1}; t_{n+1-q}))$ at the mesh points, so that interpolations/extrapolations are only needed in time. This requires to solve, with in our case the RK4 (fourth order Runge–Kutta) scheme and possibly sub-time cycling, a set of Q problems involving an advection equation.

Applying now the filtering operator we get:

$$\overline{D_t \mathbf{u}} \approx \frac{1}{\Delta t} \left(\alpha_0 \bar{\mathbf{u}}^{n+1} + \sum_{q=1}^{q=Q} \alpha_q \bar{\tilde{\mathbf{u}}}^{n+1-q} \right)$$

Then the closure problem consists in determining the $\bar{\tilde{\mathbf{u}}}^{n+1-q}$ from the $\bar{\mathbf{u}}^{n+1-q}$. To do that, we use an ADM type approach, i.e. we introduce an approximate inverse of the filtering operator. The algorithm proposed in [4,12] can be written:

$$\bar{\tilde{\mathbf{u}}}^{n+1-q} = (1 + G(T - 1)G^+) \bar{\mathbf{u}}^{n+1-q}$$

where G denotes the filtering operator, G^+ the approximate inverse of G and $T(\mathbf{u})$ the transport operator such that $\tilde{\mathbf{u}}^{n+1-q} = T \mathbf{u}^{n+1-q}$. Let us remark that the straightforward approach, $\bar{\tilde{\mathbf{u}}}^{n+1-q} = G T G^+ \bar{\mathbf{u}}^{n+1-q}$, yields a non-consistent algorithm. Indeed, in the limit $\Delta t = 0$, for which $T = 1$, we have $G G^+ \neq 1$. The choice of the operators G and G^+ is, of course, crucial. In the framework of a Fourier–Chebyshev spectral method, it of interest to apply the filtering operations in Fourier space, where the convolution products return to being simple products. In fact, we use for G and G^+ quadratic approximations of the Gaussian filter and of its inverse, as shown in Fig. 1, but in order to avoid the meaningless negative values of the G -spectrum, we cancel them in the higher wave-number range (G' -spectrum).

2.2. Diffusion step and SVV stabilization

In the diffusion step one computes a provisional velocity such that:

$$\left(\frac{1}{Re} \nabla^2 + S - \frac{\alpha_0}{\Delta t} \right) \mathbf{u}^* = \mathbf{s}^{n+1} \quad \text{in } \Omega \tag{3}$$

$$+B.C., \quad \text{e.g. } \mathbf{u}^*|_{\Gamma} = \mathbf{u}^{n+1}|_{\Gamma} = \mathbf{u}_{\Gamma} \tag{4}$$

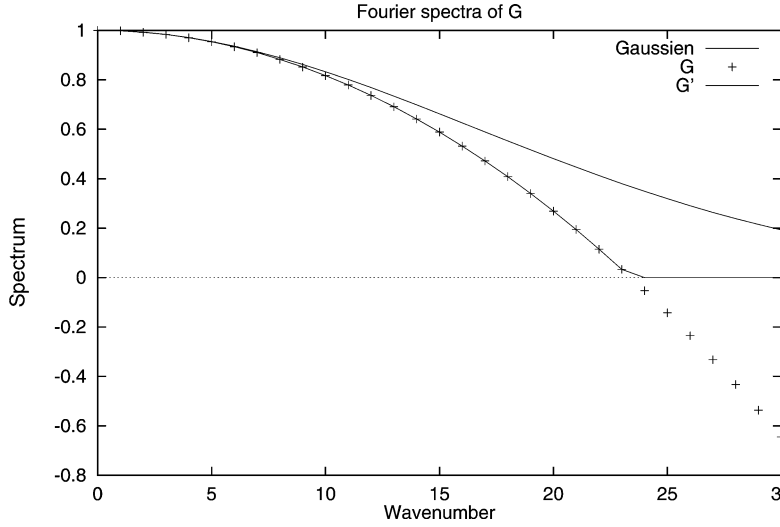


Fig. 1. Spectra of the Gaussian filter and of its approximations G and G' . The (non-plotted) spectrum of G^+ is symmetric to that of G .

where S is the SVV stabilization operator and where:

$$s^{n+1} = \frac{1}{\Delta t} \sum_{q=1}^{q=Q} \alpha_q \tilde{u}^{n+1-q} + \nabla p^* - f^{n+1}$$

with p^* a provisional pressure. In the framework of a second order implementation: $Q = 2$ and $p^* = p^n$ (the ‘Goda scheme’ [16]).

Our definition of the SVV operator S relies on that introduced in [9] for the resolution, in the interval $(-1, 1)$, of 1D hyperbolic equations by using the spectral Legendre method. In this case, with N for the degree of the polynomial approximation, we have:

$$Su := \epsilon_N \partial_x Q(\partial_x u)$$

where Q is the operator such that, with L_k the Legendre polynomial of degree k :

$$Q\phi \equiv \sum_{k=0}^N \hat{Q}_k \hat{\phi}_k L_k, \quad \forall \phi, \quad \phi = \sum_{k=0}^N \hat{\phi}_k L_k$$

with $\epsilon_N = O(N^{-1})$, $\hat{Q}_k = 0$ if $k \leq m_N$ and $1 \geq \hat{Q}_k > 0$ if $k > m_N$. Typical choices for m_N are $m_N = O(\sqrt{N})$ [9] or $m_N = N/2$ [17]. For $m_N < k \leq N$ the numerical experiments show that a smooth variation for \hat{Q}_k yields better results. Thus, as in [9] we will use:

$$\hat{Q}_k = \exp\left(-\left(\frac{N-k}{m_N-k}\right)^2\right), \quad k > m_N$$

In our multidimensional framework, such a SVV term may be extended in:

$$Su_i^* := \epsilon_N \nabla \cdot Q(\nabla u_i^*)$$

with u_i^* any component of u^* and where Q applies independently to each component of ∇u_i^* . Let us remark that such an extension of the initial 1D definition may be discussed, especially when complex geometries are considered [18]. Let us also mention that with L a characteristic dimensionless length of the computational domain (subdomain in our case) then, from scaling arguments, $\epsilon_N = O(L/(2N))$.

2.3. Projection step

To derive from \mathbf{u}^* a divergence-free velocity field \mathbf{u} , we solve the *Darcy problem*:

$$\begin{aligned}\mathbf{u}^{n+1} + \nabla\varphi &= \mathbf{u}^* & \text{in } \Omega \\ \nabla \cdot \mathbf{u}^{n+1} &= 0 & \text{in } \Omega \\ \mathbf{u}^{n+1} \cdot \mathbf{n}|_{\Gamma} &= \mathbf{u}_{\Gamma} \cdot \mathbf{n}\end{aligned}$$

and then update the pressure field $p^{n+1} = p^n + \alpha_0\varphi/\Delta t$.

Solving the above Darcy problem is not straightforward. Following [19,20] we use a *unique grid* $P_N - P_{N-2}$ strategy. Essentially, this means that the polynomial spaces of the pressure and of the velocity components are chosen different, so that no boundary conditions are required for the pressure which is completely defined by its values at the inner grid-points. Thus, in the monodomain case, the polynomial interpolant of the pressure is 2 degrees less than for the velocity components in the non-homogeneous directions. Some details on the multidomain case are given in [12].

3. Turbulent wake of a cylinder ($Re = 3900$)

As e.g. in [21] we are interested in the computation of the turbulent wake of a cylinder at a Reynolds number (based on the diameter and on the mean flow velocity) of $Re = 3900$. Moreover, the Navier–Stokes equations are solved together with a transport–diffusion equation for the temperature, without coupling, i.e. the temperature essentially behaves as a passive scalar.

With x, y, z for the longitudinal, cross-flow and spanwise directions, respectively, the computational domain is $\Omega = (-6.5, 17.5) \times (-4, 4) \times (-2, 2)$, and the cylinder is of unit diameter with axis at $x = y = 0$.

The initial and boundary conditions are, in dimensionless form: (i) at $t = 0$, fluid at rest ($\mathbf{u}(t = 0) = 0$) and thermally stratified ($T(t = 0) = y$) and (ii) Dirichlet conditions at the inlet ($\mathbf{u}(x = -6.5) = 1$, $T(x = 0) = y$), free-slip conditions for \mathbf{u} and adiabaticity conditions for T at the horizontal boundaries ($y = \pm 4$), soft outflow boundary conditions (see [11]) at the outlet ($x = 17.5$).

The calculations have been carried out with the following spatial approximation: number of subdomains in x -direction $S = 5$, Chebyshev polynomial degree in x and y , $N_1 = 60$ and $N_2 = 120$ respectively, number of Fourier-grid points in z , $N_F = 60$. We have used a time-step $\Delta t = 5 \times 10^{-3}$ without sub-cycling in the transport step. For the SVV parameters we chose $\epsilon_N = 1/N$ and $m_N = \sqrt{N}$.

Visualizations at a given time of the 3D flow computed with the SVV method are shown in Fig. 2. At left the isotherms $T = \pm 1.5$ are visualized and at right it is the Q criterion (see e.g. [22]). The streamwise and spanwise

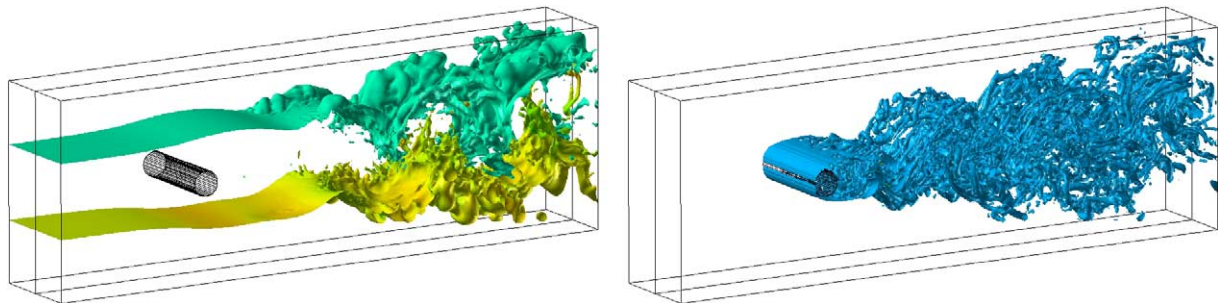


Fig. 2. Isotherms (left) and Q criterion (right) with SVV.

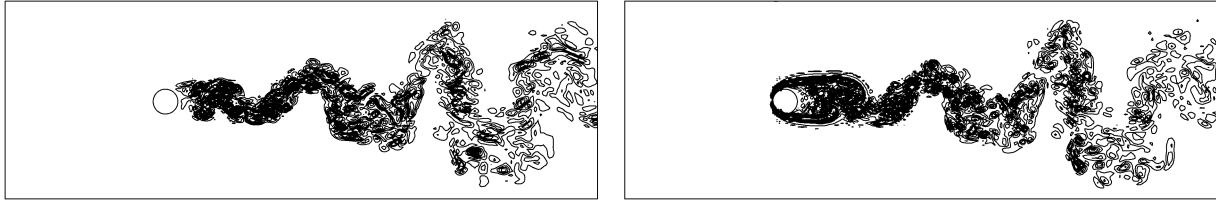


Fig. 3. Streamwise (left) and spanwise (right) components of the vorticity with SVV.

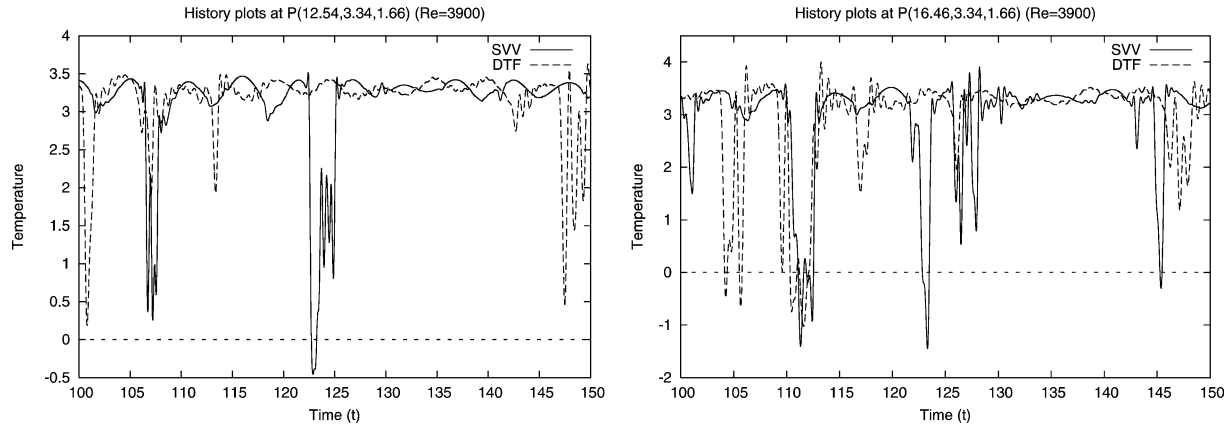


Fig. 4. $T(t)$ for DTF and SVV; $P = (12.54, 3.34, 1.66)$ (left), $P = (16.46, 3.34, 1.66)$ (right).

components of the vorticity, as computed with the SVV method, are shown in Fig. 3. Quite similar results are obtained when using the DTF algorithm associated to the SVV method for stabilization (see [12] for such qualitative comparisons).

In Fig. 4 the time variations of the temperature at two ‘boundary points’ of the wake, as computed with the SVV and DTF algorithms, are presented. Large departure of the temperature may be observed, corresponding to the crossing of some larger eddies at these specific points. Hereafter we present more quantitative results. Firstly we examine mean velocity profiles and secondly the power spectra obtained from the evolution of the velocity components at some particular points of the flow. The results are given for computations made with the SVV stabilization technique, with the DTF-SVV algorithm and also with the SVV method when adding some noise at the inlet (‘SVV + noise’). To this end, a white noise of amplitude 0.005 is added to the y and z components of the inflow velocity. Our goal is both to check the validity of our calculations and to provide detailed comparisons of the SVV, DTF-SVV and SVV + noise results.

3.1. Mean profiles

The mean profiles have been computed from time $t = 75$, at which the turbulent flow may be considered as established, to time $t = 150$, i.e. on a time interval corresponding approximately to 15 shedding periods. Fig. 5 shows the variation of the velocity mean streamwise component along the x -axis. The right part of the figure gives a zoom of the recirculation zone. First it should be mentioned that this recirculation zone appears longer than that observed in the experiments, or in other computations [21,23]. From our point of view, this may directly result from the fact that the height of our computational domain only equals 8, which is not enough to make comparisons with results obtained in an open (or quasi-open) domain. However, one remarks from [21,23] that higher order methods seem to yield a longer recirculation zone. Secondly, one observes that the discrepancies between our three computations, SVV, DTF-SVV and SVV + noise are not important. Thus, the DTF result lies approximately

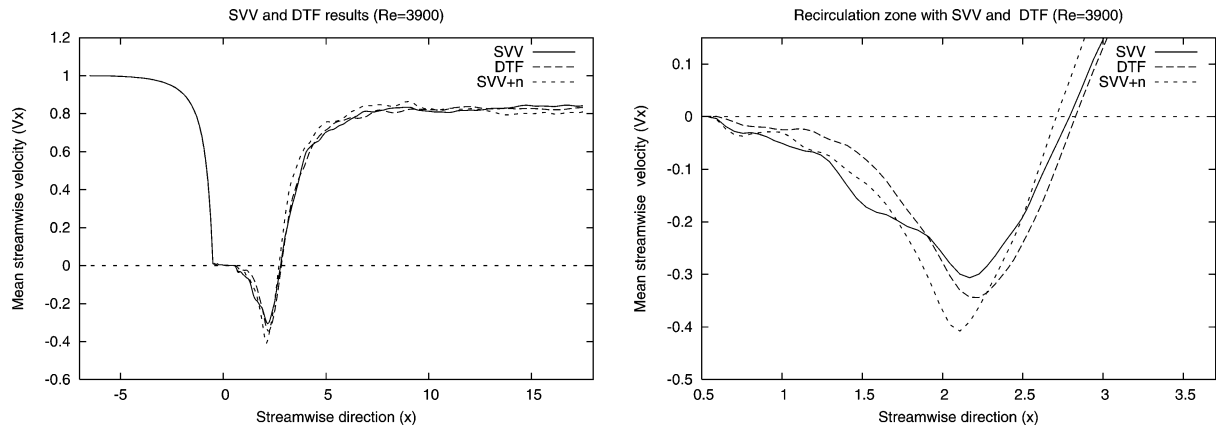


Fig. 5. $(\bar{u}_x)(x)$, along $y = z = 0$ (DTF, SVV and SVV + n).

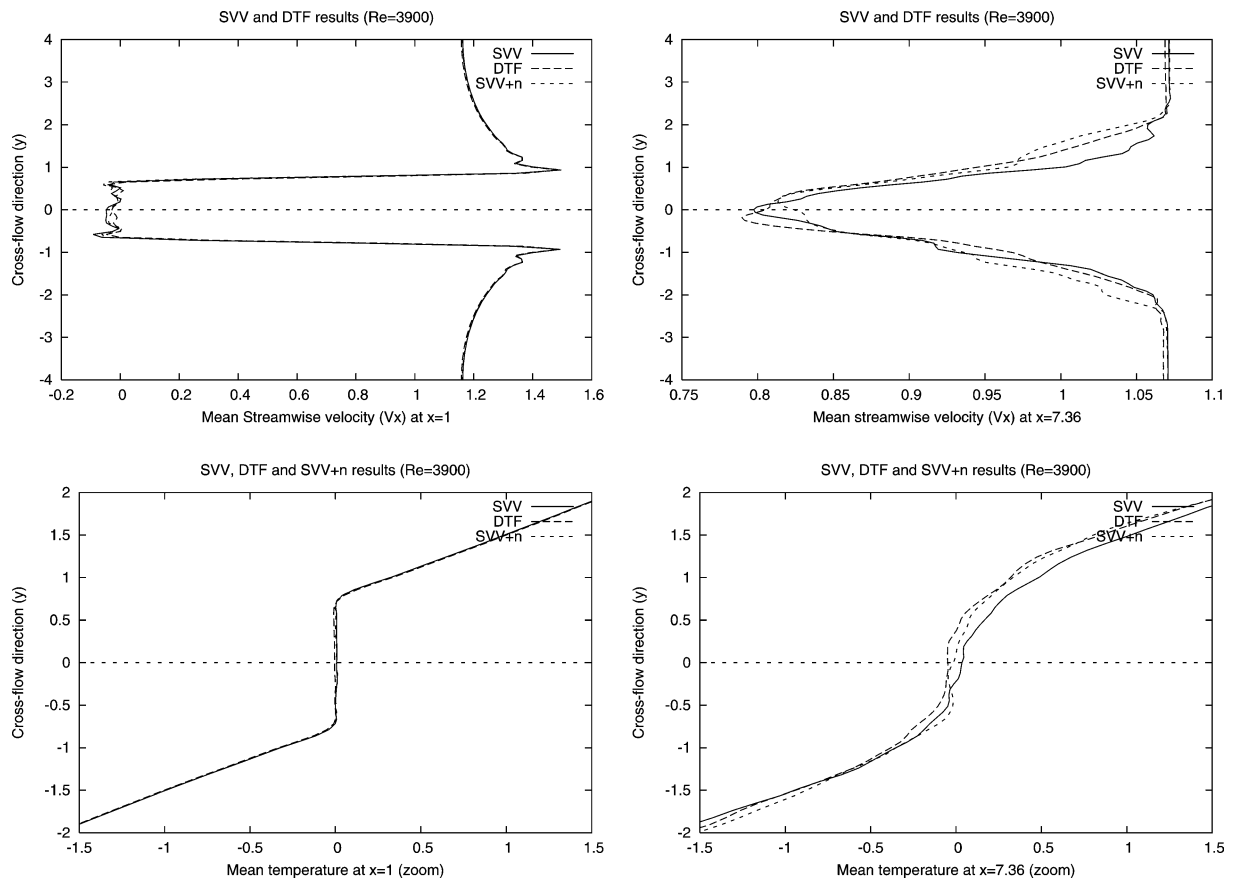


Fig. 6. $(\bar{u}_x)(y)$ (top) and $\langle T \rangle(y)$ (bottom) for $x = 1$ and $x = 7.36$ ($z = 0$) (DTF, SVV and SVV + n).

between those of SVV and SVV + noise. Mean streamwise velocity profiles are shown in Fig. 6. The left one is located in the recirculation zone, and the right one downflow. Zooms of the corresponding temperature profiles are

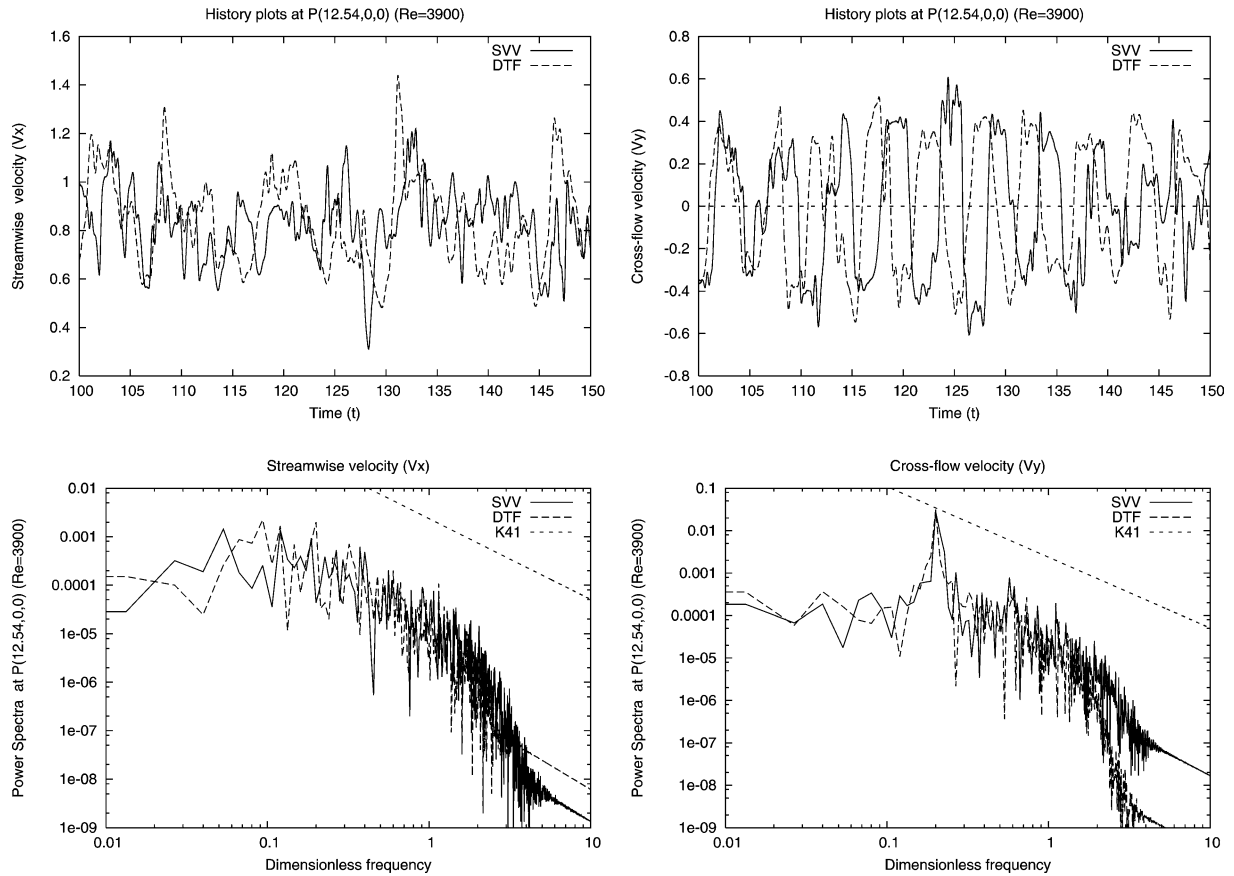


Fig. 7. $u_x(t)$ (left), $u_y(t)$ (right) and corresponding spectra for DTF and SVV; $P = (12.54, 0, 0)$.

also shown in Fig. 6. Here again one observes that the three computations yield similar results, especially close to the cylinder. Downflow, one may assume that the small discrepancies that can be observed essentially result from a not enough long averaging time, as pointed out by some lack of symmetry of the profiles.

3.2. Power spectra

In order to go into the details of the LES modeling, one has to analyze the frequency content of the velocity field. For inhomogeneous flows, it is convenient to proceed as in experiments, from time evolutions of the velocity components at different points. Through the Taylor hypothesis one can then produce power spectra representative of the distribution of the turbulent kinetic energy in wavenumber space, and then compare it to the Kolmogorov law describing the inertial range. This gives again a way to compare the results obtained with the SVV, DTF-SVV and SVV + noise computations. In Fig. 7 are compared the time variations at a given point of the x - and y -components of the velocity, computed with SVV and DTF-SVV. The corresponding power spectra are also presented and compared with the $k^{-5/3}$ slope of the Kolmogorov theory. Essentially one observes that the dimensionless shedding frequency (the Strouhal number) approximately equals 0.2 and that the power spectra show the expected behavior in one part of the spectrum, before decreasing faster in a numerical dissipation frequency range. Also, one clearly observes that this dissipation range is slightly larger for the DTF-SVV than for the SVV computations. The filtering part of the DTF algorithm is certainly responsible for this behavior.

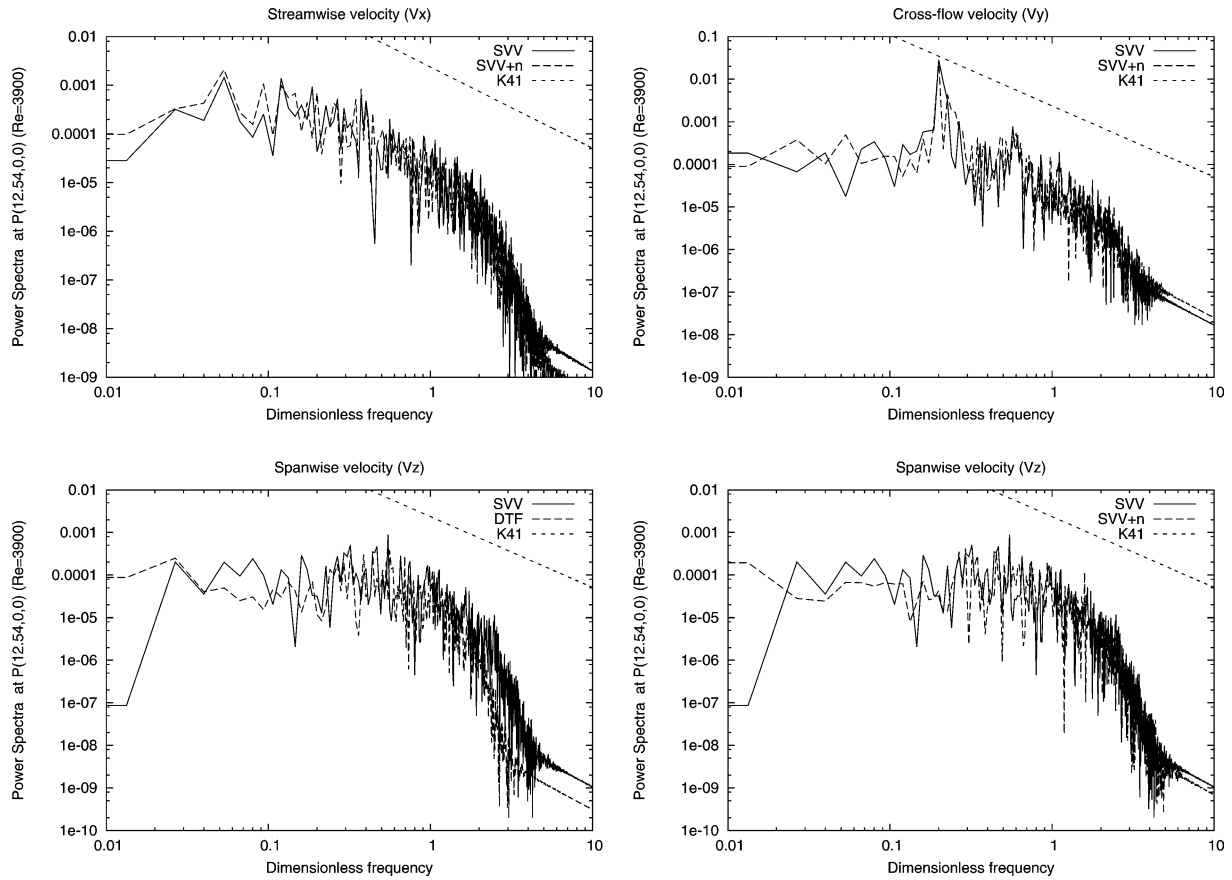


Fig. 8. Top: u_x (left) and u_y (right) power spectra for SVV and SVV + noise; $P = (12.54, 0, 0)$; Bottom: u_z power spectra for SVV and DTF (left) and for SVV and SVV + noise (right); $P = (12.54, 0, 0)$.

Power spectra obtained for SVV and SVV + noise are plotted in Fig. 8. This figure also shows the power spectra obtained for the z -component of the velocity, using SVV, SVV-DTF and SVV + noise. One observes similar results for this component of the velocity, except maybe that the inertial range appears to be slightly smaller.

4. Comments

The striking point of the present study is that the no-model approach, making use only of the stabilization technique, and the ADM type DTF modeling have yielded very similar results. This may be due to the choice of the SVV tuning parameters, ϵ_N and m_N . In particular, the SVV activation parameter m_N was chosen small ($m_N = \sqrt{N}$). It remains that the no-model approach has yielded satisfactory results, especially when looking at the power-spectra. Moreover, in the high frequency range, the no-model approach appears better than the DTF one.

Nevertheless, it is expected that taking into account the sub-grid scale contributions to the flow, improves the LES modeling. In the framework of ADM approaches, the choice of the filtering and defiltering operators may be important. In particular, our conviction is that the ADM can only result in some non-controlled noise for the SGS model contribution if it is not associated with a two-level grid approach, (see e.g. [24]). Thus, for the DTF algorithm, one may think, if necessary, to represent the defiltered quantities on a finer grid than the filtered ones. In this spirit, using the filter G' (see Fig. 1), whose spectrum vanishes beyond a critical wavenumber, say k_c , is,

from our point of view, fully justified. Using such a filter is clearly close to using a two-level grid technique, with the advantage of the higher flexibility offered by the fact of working in spectral space than working in physical space. Thus, for fully periodic problems, the filtered quantities would not show spatial frequencies beyond k_c , and it is only during the transport step, in which the non-linear convective term is taken into account, that the full frequency range would be used to handle the defiltered quantities. In the framework of a two-level grid approach, the high wave-number range should be disregarded, since we are only interested in the computation of the filtered quantities. As a result, the fact that with the DTF method the power spectra are slightly worse in the high frequency range than with the no-model approach should also be disregarded. However, it remains that our present choice of the filtering and defiltering operators can certainly be improved.

Our LES modeling is fully explicit, in the sense that the filtering (and defiltering) operation is explicitly applied. To this end, we work in spectral space, both for the Fourier and for the Chebyshev approximations. In case of the Chebyshev approximation this corresponds to apply a filter of constant width to the 2π -periodic function $u(-\cos(z))$, $z \in R$, i.e. to first map the Gauss–Lobatto–Chebyshev grid to a regular grid and then to extend it, first by symmetry and then by periodicity. This procedure is close to that suggested in [25], where the filtering operation, in case of non-equidistant grid-points, is defined by a mapping from the computational domain to the real axis. Moreover, such a procedure may be extended to meshes different from the Chebyshev–Gauss–Lobatto mesh, as soon as there exists a smooth, even and 2π -periodic mapping to similarly associate a Fourier type grid to the computational grid (1D case).

5. Conclusions

Two variants of a high-order LES model have been described and then compared, by computing the wake of a cylinder at Reynolds number $Re = 3900$. The first makes only use of the SVV stabilization technique, which shows the essential property to preserve the exponential convergence of the spectral approximation. This approach may be classified as a no-model approach, in the sense that modeling the SGS tensor is not attempted. On the other hand, the second combines an ADM type approach (the DTF algorithm in the frame of our semi-Lagrangian method) and the SVV stabilization technique. Both quantitatively and qualitatively, satisfactory and very similar results have been obtained. The power spectra, especially, show a behavior in agreement with Kolmogorov theory over a large wavenumber range.

Acknowledgements

The computations were made on the NEC-SX5 computer of the IDRIS computational center (project 024055). We are grateful to J.M. Lacroix, engineer of the CNRS, for his helpful contribution, especially for the fluid flow visualizations.

References

- [1] B.J. Geurt, Inverse modeling for large-eddy simulation, *Phys. Fluids* 9 (12) (1997) 3585–3587.
- [2] S. Stolz, N.A. Adams, An approximate deconvolution procedure for large-eddy simulation, *Phys. Fluids* 11 (7) (1999) 1699–1701.
- [3] J. Bardina, J.H. Ferziger, W.C. Reynolds, Improved turbulence models based on large eddy simulation of homogeneous incompressible turbulence, Stanford University, Report TF-19, 1983.
- [4] R. Pasquetti, C.J. Xu, High-order algorithms for large eddy simulation of incompressible flows, *J. Sci. Comput.* 17 (1–4) (2002) 273–284.
- [5] P. Sagaut, *Introduction à la simulation des grandes échelles pour les écoulements de fluide incompressible*, Mathématiques & Applications, Springer, 1998.
- [6] M. Germano, U. Piomelli, P. Moin, W.H. Cabot, A dynamic sub-grid scale eddy viscosity model, *Phys. Fluids* 3 (7) (1991) 1760–1765.
- [7] T.B. Gatsky, M.Y. Hussaini, J.L. Lumley, Simulation and modeling of turbulent flows, in: J.H. Ferziger (Ed.), *ICASE/LaRC Series in Computational Science and Engineering*, Chapter 3, Large Eddy Simulation, 1996, pp. 109–154.

- [8] E. Tadmor, Convergence of spectral methods for nonlinear conservation laws, *SIAM J. Numer. Anal.* 26 (1) (1989) 30–44.
- [9] Y. Maday, S. Kaber, M. Ould, E. Tadmor, Legendre pseudo-spectral viscosity method for nonlinear conservation laws, *SIAM J. Numer. Anal.* 30 (2) (1993) 321–342.
- [10] M. Lesieur, O. Métais, New trends in large-eddy simulation of turbulence, *Annu. Rev. Fluid Mech.* 28 (1996) 45–82.
- [11] M.Y. Forestier, R. Pasquetti, R. Peyret, Computations of 3D wakes in stratified fluids, in: *Computational Fluid Dynamics Conference ECCOMAS 2000*, 2000, proc. in CD.
- [12] L. Cousin, R. Pasquetti, High-order methods for the simulation of transitional to turbulent wakes, in: Y. Lu, W. Sun, T. Tang (Eds.), *Third Int. Workshop on Scientific Computing and Applications*, City University Hong-Kong, 6–9 January 2003, in: *Advances in Scientific Computing and Applications*, Science Press, Beijing, New York, 2004, pp. 133–143.
- [13] Y. Maday, A.T. Patera, E.M. Ronquist, An operator-integration-factor splitting method for time-dependent problems: application to incompressible fluid flow, *J. Sci. Comp.* 5 (4) (1990) 263–292.
- [14] R.M. Phillips, T.N. Phillips, Flow past a cylinder using a semi-Lagrangian spectral element method, *Appl. Numer. Math.* 33 (2000) 251–257.
- [15] C.J. Xu, R. Pasquetti, On the efficiency of semi-implicit and semi-Lagrangian spectral methods for the calculation of incompressible flows, *Int. J. Numer. Methods Fluids* 35 (2001) 319–340.
- [16] K. Goda, A multistep technique with implicit difference schemes for calculation two and three dimensional cavity flows, *J. Comput. Phys.* 30 (12) (1979) 76–95.
- [17] G.S. Karamanos, G.E. Karniadakis, A spectral vanishing viscosity method for large-eddy simulation, *J. Comput. Phys.* 163 (2000) 22–50.
- [18] C.J. Xu, R. Pasquetti, Stabilized spectral element computations of high Reynolds number incompressible flows, *J. Comput. Phys.* 196 (2004) 680–704.
- [19] M. Azaiez, A. Fikri, G. Labrosse, A unique grid spectral solver of the nD Cartesian unsteady Stokes system. Illustrative numerical results, *Finite Elem. Anal. Design* 16 (3–4) (1994) 247–260.
- [20] O. Botella, On the solution of the Navier–Stokes equations using Chebyshev projection schemas with third order accuracy in time, *Computers & Fluids* 26 (2) (1997) 107–116.
- [21] A.G. Kravchenko, P. Moin, Numerical studies of flow over a circular cylinder at $Re = 3900$, *Phys. Fluids* 12 (2) (2000) 403–417.
- [22] J. Jeong, F. Hussain, On the identification of a vortex, *J. Fluid Mech.* 285 (1995) 69–94.
- [23] R.P. Hansen, L.N. Long, Large-eddy simulation of a circular cylinder on unstructured grids, in: *Proc. of 40th AIAA Aerospace Sciences Meeting and Exhibit*, 14–17 January 2002.
- [24] J.A. Domaradzki, E.M. Saiki, A subgrid-scale model based on the estimation of unresolved scales of turbulence, *Phys. Fluids* 9 (7) (1997) 2148–2164.
- [25] S. Ghosal, P. Moin, The basic equations for the large-eddy simulation of turbulent flows in complex geometry, *J. Comput. Phys.* 118 (1995) 24–37.